Imaging pollen using a Raspberry Pi and LED with deep learning

Ben Mills [1], Michalis N Zervas [1] and James A Grant-Jacob [1,*]

Optoelectronics Research Centre, University of Southampton, Southampton, SO17 1BJ, UK.

*Corresponding author: J.A.Grant-Jacob@soton.ac.uk;

Highlights

1. Current methods of pollen sensing are bulky and expensive.
2. An LED and Raspberry Pi are used to reduce the cost of sensing.
3. Lensless imaging and deep learning are used to image pollen grains.
4. Pollen grains images were generated from their scattering patterns.
5. Imaging pollen using a Raspberry Pi, LED and deep learning can be achieved for ~£100.

Keywords

AI, Imaging, Palynology, Bioaerosols, Sensing, Pollen grains

Abstract

The production of low-cost, small footprint imaging sensor would be invaluable for airborne global monitoring of pollen, which could allow for mitigation of hay fever symptoms. We demonstrate the use of a white light LED (light emitting diode) to illuminate pollen grains and capture their scattering pattern using a Raspberry Pi camera. The scattering patterns are transformed into 20× microscope magnification equivalent images using deep learning. We show the ability to produce images of pollen from plant species previously unseen by the neural network in training. Such a technique could be applied to imaging airborne particulates that contribute to air pollution, and could be used in the field of environmental science, health science and agriculture.

1 Introduction

Pollen allergies, also known as hay fever, are a significant health concern, affecting an estimated 26% of adults in the UK [1], with prevalence been shown to be increasing in Denmark over the past 20 years [2], and economic cost being €195.6 patient/year in China [3] These allergies can have a substantial impact on an individual's health, especially during the spring and summer months [4]. Whilst only specific pollen producing plants cause hay fever, the local pollen count can aid in the mitigation of hay fever symptoms, as it gives an indication of potential levels of overall pollen in the air. However, these counts generally do not consider pollen of plant species, which can have degrees of allergenicity [5,6]. Therefore, the development of a real-time sensor that can identify and quantify pollen of different plant species at a specific location would be extremely beneficial. Whilst the plant species that produce pollen that can lead to hay fever is still unclear [7], and individuals suffering from hay fever should seek medical advice to discover more about their allergies, such a device could aid individuals in identifying the specific plant taxa causing their severe symptoms or even avoid exposure to these pollens. In addition to its health benefits, monitoring pollen levels can also provide valuable information about the climate [8], insect migration patterns [9], and crop production [10].

Currently, the techniques available for real-time sensing of pollen grains are limited in temporal and spatial resolution. Whilst optical particle counters can detect particles of a certain size in real-time, they cannot identify the species of particle (i.e., smoke, pollen, cement dust) [11]. Pollen collected using Burkard traps [12] (kettle-sized traps or larger depending on type) requires subsequent laboratory analysis to determine the family or species [13]. Some analysis techniques can identify pollen up to plant species level whereas others do not come further than family or genus. Light microscopy techniques often only allow identification up to the family or genus level, since many pollen grains have similar morphological characteristics, making it difficult to distinguish between species within the same family or genus.

Acetolysis is a technique used to process pollen and prepare it for morphological identification via light microscopy [14], by removing unwanted substances from the grains, revealing important morphological features of the grains. Pollen grains can also be stained prior to light microscopy analysis to allow better contrast with the background, providing greater detail of the exine and ornamentation [15]. FTIR (Fourier Transform Infrared Spectroscopy) is a method that uses infrared light to observe chemical properties of pollen grains and can help in distinguishing between different taxa, and even species in some cases [16]. Another method, DNA Metabarcoding utilises DNA extraction, sequencing, and analysis for plant species level identification of pollen [17].

Recently, automated methods for identifying pollen from traps have been developed using light-based techniques such as optical and laser-based fluorescence imaging [18–21]. However, these devices can be quite large, and so a sensor capable of imaging a pollen grain with cost-effective and minimal optics, and with a small footprint (such as a lensless-based Raspberry Pi [22]) would be invaluable for mass deployment in practice on a national or international scale. A method that uses minimal optics is lensless imaging, which images via capturing and processing the light scattered from an object (i.e., the image of its scattering pattern). This scattering pattern image contains information about the object's morphology and chemical composition [23,24], and can be converted into an image of the sample using methods such as phase retrieval and ptychography [25–27], or more recently using deep learning neural networks [28–31].

The capability of airborne imaging of pollen would allow plant pollen family verification, and identification of the size and shape of pollen (all of which are useful for understanding crop health and the environment). For example, a study suggests that pollen grain size could potentially be used as a proxy for long-term climate change [32], particularly in relation to changes in moisture availability. Another study found that both soil fertility and mycorrhizal infection had significant effects on the male traits of

the plants, including pollen production and pollen grain size [33], suggesting that changes in the environment, such as nutrient availability in the soil, could influence the characteristics of pollen.

Whilst deep learning CNNs have been also successful in identifying pollen from scattering patterns [34,35], these works involve the use of CNNs for identification and not for image generation. The setups in the papers included the use of expensive imaging cameras (~£500 each) to capture the scattering patterns, and so a cheaper camera such as a Raspberry Pi camera (~£50) would be more desirable. In addition, these previous works used lasers for creating scattering patterns in lensless imaging, but a cheaper light source like an LED (light emitting diode) could enable even lower cost sensing (potentially 100× lower cost for the light source). In general, lasers are used for lensless imaging due to their higher spatial coherence, which provides diffraction patterns with structure that the deep learning neural networks can interpret. In this work, we use a white light LED coupled with an aperture (for spatial filtering of the light), to produce a scattering pattern from the pollen grains onto a Raspberry Pi camera sensor and subsequently use deep learning to transform that scattering pattern into an image of the pollen grain. Different from CNNs, we use a conditional generative adversarial network (cGAN), which rather than reduces an image to a single or vector output, such architecture is a U-net structure such that it reduces the image, but then increases it again to an image the same size as the input, transforming it in the process. The ability to link a scattering pattern from a pollen grain to its microscope image negates the need to produce microscope images, thus significantly reducing costs and saving time. Critically, the ability to image a pollen grain can allow for shape, size, and colour of the pollen grains to be determined, in addition to identification of the species producing the pollen.

2 Materials and Methods

2.1 Sample preparation

The taxa used in this experiment were pollen that had a variety of shapes and sizes (to allow the neural network to learn from a diverse dataset) and were available on the university campus or available to order. *Iva xanthiifolia* and *Populus deltoides* pollen grains were procured from Sigma Aldrich. *Allium ursinum*, *Narcissus pseudonarcissus*, *Tulipa saxatilis*, *Ranunculus repens* and *Taraxacum officinale* pollen grains were collected from the University of Southampton grounds. From this point forward, we shall only use the genus of the plant for ease of reading. Two substrates (25 mm × 75 mm × 1 mm thick pre-cleaned soda-lime glass slide by J. Melvin Freed Brand) were used. These glass slides were cleaned using acetone and lens tissue, and allowed to dry before pollen from each species was sequentially deposited onto them using a laboratory grade cotton bud (RS.com). The pollen grains were sprinkled over the surface of the glass slide, covering approximately a 25 mm × 25 mm area, at a density of ~3 pollen per mm^2. The pollen used were dry and did not contain any staining chemicals, nor was acetolysis used. *Iva*, *Populus*, *Narcissus* and *Ranunculus* pollen grains were deposited onto the first substrate (for neural network training and testing), whilst *Tulipa*, *Allium* and *Taraxacum* pollen grains were deposited onto the second substrate (for neural network testing only).

2.2 Experimental setup

The experimental setup is presented in figure 1a). To image the pollen grains, we used a Nikon ECLIPSE LV150L with a 20× Nikon objective (NA = 0.4, WD = 13 mm), a 10× ocular lens, a 0.55× TV lens and a colour camera (Basler acA3088-57uc, 6MP IMX178 sensor, 3088 × 2064 pixels, RGB), giving a 110× total image magnification. A pollen covered glass slide was attached to motorized XYZ Zaber stages that could translate the pollen beneath the microscope in a raster scanning motion in X and Y to acquire images, and could then translate to the Raspberry Pi scattering setup. The step size of the X and Y stages was 0.047 µm, having an accuracy of 15 µm, repeatability of <3 µm. The Raspberry Pi setup illumination/scattering Z-axis was approximately 85 mm away from the centre of the microscope imaging Z-axis. This combination

of two adjacent experimental systems allowed the collection of both microscope images of the sample and the associated scattering patterns, which was key for training the neural network to transform scattering patterns into microscope images. However, it is important to realise that whilst two systems were used here, once the neural network is trained, only the low-cost Raspberry Pi sensor system would be needed for in practice implementation. As demonstrated in previous work, the Raspberry Pi itself could also run the trained neural network [36]. This means that one can duplicate the Raspberry Pi setup for capturing scattering patterns, and transform the scattering patterns into microscope images without the need for an expansive microscope (~£10,000), or even microscope objectives (~£1000) to image the pollen grains.

The Raspberry Pi sensor setup consisted of a white light LED. The LED was followed by an aperture (<1mm diameter) placed approximately 2 cm after the end of the LED to spatially filter the light from the LED, and therefore enhance the fringe visibility in the scattering patterns, hence enhancing the likelihood of a neural network being able to transform a scattering pattern image correctly into an image of the pollen grain. Following this, the light was focussed onto a pollen grain using a moulded plastic aspheric lens (6 mm, NA=0.38), and the light scattered from the pollen grain was then captured using an HQ Pi camera (4056 × 3040 pixels, RGB), which was connected to a Raspberry Pi 4. The Raspberry Pi scattering setup cost approximately £100.

Data from the Raspberry Pi camera were acquired remotely via an ethernet cable connected to a Dell Precision 7865 Windows 10 workstation consisting of an Intel(R) Xeon(R) Gold 5222 CPU @ 3.80GHz 3.79 GHz (2 processors) and 3× NVIDIA RTX A4500 (20 GB VRAM, 184 tensor cores each) graphics processing unit (GPU). The workstation also controlled the Zaber XYZ stages and the microscope's Basler camera. The stages and imaging of both the Basler and Pi cameras was automated using Python code.

2.3 Data collection

The first sample was raster scanned using XYZ stages (Zaber X-LSM050A-E03, X-LSM100A, X-VSR20A-E01) beneath the objective over a total of approximately 500 mm^2. Each raster scanning step was 550 microns to minimise any overlapping of images and minimise the time of data collection. Individual and agglomerated pollen grains were located and imaged such that each pollen grain was at the centre of the camera sensor, after which the images were cropped. The corresponding scattering patterns were collected for training and testing of the neural network. The images of the scatting patterns were cropped to 1024 × 1024 pixels then resized to 256 × 256 pixels to match the size of the cropped microscope images. Subsequently, the pollen grains from the second slide were imaged and scattering patterns were recorded, purely to test the capability of the neural network to generate images of not just unseen pollen grains but pollen grains from previously unseen plant species. In total, 1800 images were collected, but agglomeration of pollen grains that extended beyond the cropped and resized 256 x 256 pixels image size were discarded. As such, 935 pairs of images (microscope image and scattering pattern) were used for training and 31 used for testing from the first slide with 100 used for testing from the second slide.

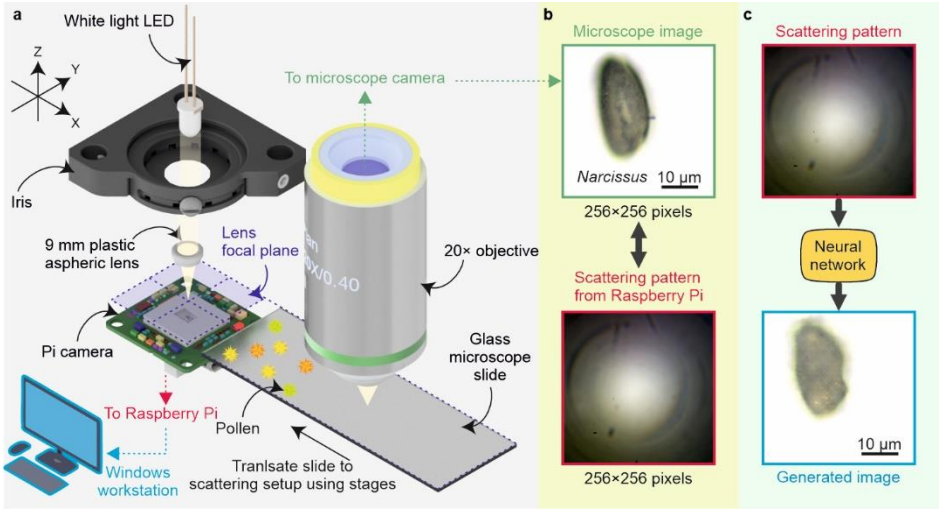

Fig. 1. A) Diagram of experimental setup showing the imaging setup consisting of a 20× microscope objective connected to a microscope, next to the Raspberry Pi-based sensing setup. The pollen covered

glass microscope slide was translated between setups using motorised XYZ stages. B) Example of a microscope image (green outline) from the imaging setup and associated scattering pattern (red outline) captured by the Pi camera from the sensing setup. c) Schematic of transforming scattering pattern (red outline) using a neural network (yellow box), trained on a Windows workstation, into a generated image of the pollen grains (blue outline).

A total of 935 pollen images and scattering patterns (divided over 4 different species, *Iva*, *Populus*, *Narcissus* and *Ranunculus*) from the first slide were used to train the neural network (see table 1). The number of plants that *Iva* and *Populus* were collected from is unknown as they were purchased from Sigma Aldrich, but since the bottles are 1 g and 500 mg, respectively, to obtain such a quantity of pollen would require pollen to be sourced from a large quantity of flowers. Pollen was collected from 4× *Ranunculus*, 4× *Taraxacum*, 3× *Tulipa*, 3× *Allium*. However, whilst multiple flowers were collected, due to the sparsity of such pollen from the plants, the numbers used in training and testing were low. It should be noted that some pollen grains were fragmented, and blank images were also included in the data, hence have been assigned the unknown column in table 1. Even though more pollen from *Iva* were used in training, and it has been shown that a varied dataset is necessary for overfitting [37], the key part for accurate image generation is to have enough varied data, such as pollen grains of different orientation, sizes and agglomerations. The pollen size distribution of the training data was calculated by binarizing the images and calculating the white pixels that represented the pollen. This showed that pollen grains in the training set had a distribution with a mean area of 2341.8 pixels^2 (383.3 microns^2) and a standard deviation of 1757 pixels^2 (287.6 microns^2), indicating significant variability. The distribution is strongly right-skewed (skewness = 1.95) with heavy tails (kurtosis = 7.63), suggesting the presence of large outliers. A lognormal distribution with parameters $\mu = 5.24$ and $\sigma = 3.46$ provides a good fit to the data, which is typical for naturally occurring size distributions. Table 1 shows the number of pollen grains from different species used in training and testing.

Table 1 Number of pollen grains from each plant species used in training and testing the neural network.

	Ranunculus	*Populus*	*Narcissus*	*Iva*	*Tulipa*	*Allium*	*Taraxacum*	*Unknown*
Training	91	47	137	650	0	0	0	10
Testing	5	2	10	13	47	30	23	1

2.4 Neural network

Deep learning convolutional neural networks (CNNs) are designed to mimic the visual cortex and use convolutional layers to process features in images. They have proven to be very successful at identifying objects in images, and have been used in the automatic identification of pollen in images [37,38]. Unlike CNNs, we utilise a conditional generative adversarial network (cGAN) with a U-net architecture. Instead of reducing an image to a single value or vector output, this structure reduces the image and then reconstructs it to the produce another image that is the same size as the input, transforming it in the process. We used a cGAN architecture known as Pix2pix [39], using a workstation running Windows 10 and equipped with an AMD Ryzen Threadripper PRO 5975WX and two NVIDIA A6000 GPUs (48 GB VRAM). The cGAN framework described and illustrated in more detail in [40] had a generator network with a 7-layer architecture in order to enable an image resolution of 256 × 256 pixels and had a learning rate of 0.0002 and drop-out of 0.5. At the start of training, the neuron weightings for the generator were randomly initialised, meaning they encoded no information about the training data (experimental images).

196 The neural network was trained for 160 epochs until the training errors reached a minimum, which took
197 nearly 3 hours. A total of 935 pollen images and scattering patterns from the first slide were used to train
198 the neural network. The neural network was then applied to 31 scattering patterns from the first slide
199 not used in trainings. The neural network outputted generated images of pollen grains, and were
200 compared to the experimentally obtained pollen images. To further test the capability of the neural
201 network, we used 100 scattering patterns collected from pollen grains on the second slide, since no pollen
202 grains from these plant species were used in training, and therefore structures of the pollen grains would
203 not have been seen by the neural network in training. This illustrates that the neural network has not
204 overfitted to the specific scattering patterns it was trained on but has developed a generalized
205 understanding that features in the scattering patterns correspond to features in the images of pollen
206 grains, hence enabling it to accurately recognise and relate features across different examples. Therefore,
207 the successful generation of images of previously unseen pollen species demonstrates the robustness of
208 the network.

209 ## 3 Results and discussion

210 Figure 2a displays the 10 results of testing the neural network on previously unseen pollen (*Narcissus*,
211 *Populus, Iva* and *Ranunculus*,), why Fig. 2b shows the results of testing the neural network on 10 pollen
212 grains from previously unseen plant species (*Tulipa*, *Allium* and *Taraxacum*). The first row shows the
213 experimental scattering pattern, the second row shows the images generated by the neural network, the
214 third row shows the experimental image, and the fourth row shows the difference between rows two and
215 three (RGB pixel intensity in generated image minus RGB pixel intensity in experimental image). Since the
216 image has been inverted for ease of viewing, the darker pixels (low intensity pixel value) indicate regions
217 of greater error. As seen in the figure, the quantity of the pollen grains in each generated image is correct,
218 as in the case for *Iva* there being 3 in one instance, and *Populus* and *Allium* being two, and one pollen for

all the others. The orientation and size of pollen grains in the generated images are very similar, as can be seen in the difference images in the fourth row. Whilst the size and orientation are generally correct, the surface texture is generally not. This is perhaps due to the higher spatial frequency information contained in the scattering pattern not being distinguishable (and thus extractable) due to low spatial coherence of the light source.

Table 2 displays the Structural Similarity Index Measure (1 being exactly the same, 0 indicating no similarity and -1 being completely anti-correlated), Peak Signal-to-Noise Ratio (PSNR) (higher the value the more accurate the generated image), Mean Squared Error (MSE) (lower value the greater the similarity) of the generated images compared with the experimental images and Perceptual Image Quality Evaluator (PIQE), which provides a no-reference metric based on perceptual image quality (a smaller score indicates better perceptual quality.

The SSIM assesses the visual impact of image contrast, luminance and structure, and was determined using the following formula,

$$SSIM(E,G) = \frac{(2\mu_E\mu_G + C_1)(2\sigma_{EG} + C_2)}{(\mu_E^2 + \mu_G^2 + C_1)(\sigma_E^2 + \sigma_G^2 + C_2)}$$

where μ_E is the mean of E, μ_G is the mean of G, σ_E^2 is the variance of E, σ_G^2 is the variance of G, σ_{EG} is the covariance of E and G, $C_1 = (0.01L)^2$ and $C_2 = (0.03L)^2$, where L is the dynamic range of the pixel values.

[41]The PSNR equation used was,

$$PSNR = 10\log_{10}\left(\frac{max^2(E,G)}{\frac{1}{N \times M}\sum_{M,N}(E(m,n) - E(m,n))^2}\right)$$

where N and M are the total number of rows and columns of pixels in the images, *max(E,G)* is the maximum intensity value of the experimental image E and the generated image G, and m and n are the pixels in each row and column.

The mean square error (MSE) was determined by taking the average of the squared intensity differences between each pixel in the generated image (with intensity values in the 0-255 range) and the corresponding pixel in the experimental image (also with intensity values in the 0-255 range),

$$MSE = \frac{1}{N}\sum_{i=1}^{N}(G_i - E_i)^2$$

where N is the number of data points (pixels), G_i is the generated pixel value and E_i is the actual pixel value, E_{imax} is the maximum pixel value and E_{imin} is the minimum pixel value of the experimental image.

The PIQE does not have a simple, closed-form mathematical formula like the MSE, PSNR and SSIM used for full-reference methods, but instead works by analysing localized distortion such as blocking artifacts, blur and noise. We use MATLAB's in built "piqe" found in the "Image Processing Toolbox"[41].The average SSIM for all 131 test data was 0.88 for all images, whilst the PSNR are all above 27.1 and the average MSE is 835. Any artifact to the edge of the images might not be accurately reconstructed as limited information associated with this defect might not have been contained in the scattering pattern due to the size of the LED beam. It is also evident that the colour of the generated images is generally similar to that of the experimental microscope images, i.e., either yellow or grey. The SSIM value is high likely due to the large number of white pixels in the background of t images. However, it is still important to generate this background correctly. The average PIQE value was 28.96 for all images, indicating a good image quality. More specifically in Table 2, *Narcissus*, *Tulipa* and *Taraxacum* images had good quality, while *Allium* and *Populus* images had fair image quality.

The ability to image pollen could allow more precise identification and pollen morphological analysis, and such a technique could extend to other bioaerosols or airborne particulates. Since testing data was acquired remotely via an ethernet cable, this technique could be extended to using wireless technology, which the Raspberry Pi already has, and could be extended for use in real-time with the use of a flow chamber [42] or an impactor on the surface of a glass slide [43]. The low cost of the proof-of-principle imaging sensor (~£100) could be taken up by industry where costs could be reduced further.

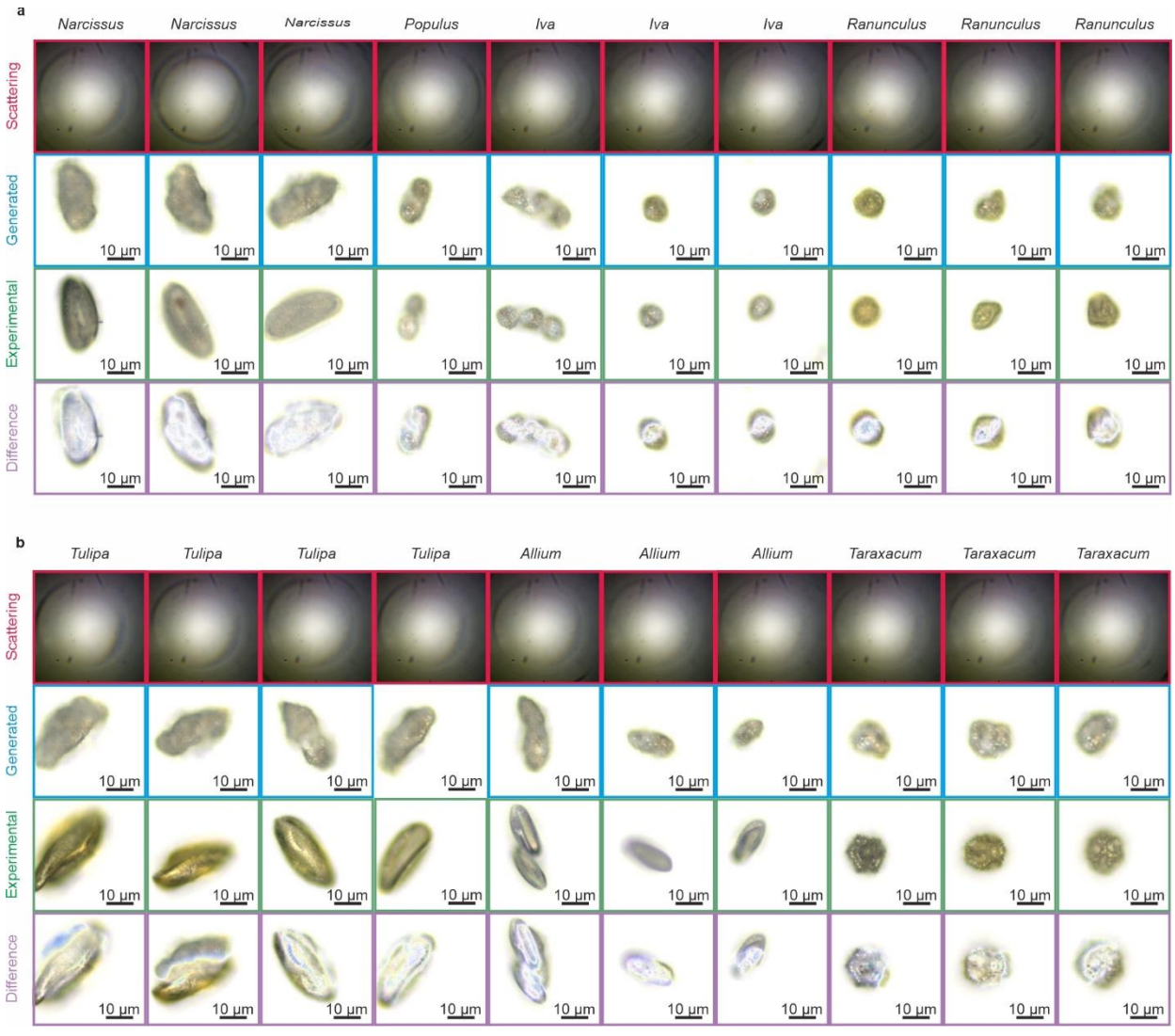

Fig. 2. Capability of the neural network on previously unseen pollen (*Narcissus Populus, Iva* and *Ranunculus*), and on previously unseen pollen from different plant species (*Tulipa*, *Alliium* and

Taraxacum). The first row shows the scattering pattern, the second row shows the generated image, the third shows the experimental image, and the fourth shows the difference, where the darker pixels indicate regions of greater error.

Table 2 SSIM, PSNR and MSE for the generated and experimental pollen images shown in Fig. 2 (the number of pollen grain images for each species is indicate in brackets).

	Ranunculus (3)	*Populus* (1)	*Narcissus* (3)	*Iva* (3)	*Tulipa* (4)	*Allium* (3)	*Taraxacum (3)*
SSIM	0.94	0.79	0.89	0.93	0.85	0.92	0.91
PSNR	23.8	12.9	22.4	24.2	18.2	23.0	21.1
MSE	274.5	3358.0	447.0	247.6	1222.5	512.8	517.9
PIQE	33.6	41.5	21.0	35.2	20.7	41.2	20.8

4 Conclusion

Using a white LED, aperture and a Raspberry Pi camera, we demonstrated the possibility of using deep learning to transform images of the LED light scattered from a pollen grain to that of an image of a pollen grain captured using a 20× magnification objective. We were able to show the reconstruction of pollen grain shape and orientation of pollen from plant species used in training such as *Populus* and *Ranunculus*, and of pollen from plant species exempt from training, such as *Tulipa* and *Allium*. The low-cost sensing technique demonstrated here could be applied to airborne pollen grains and pave the way to cheap imaging sensors for pollen and airborne particulates.

CRediT authorship contribution statement

Ben Mills: Writing – review & editing, Resources. **Michalis N Zervas**: Writing – review & editing, Funding acquisition. **James A Grant-Jacob**: Conceptualization, Methodology, Software, Formal analysis,

Investigation, Data Curation, Writing – original draft, Writing – review & editing, Visualization, Project administration.

Declaration of competing interest

The authors declare that they have no known competing financial interests or personal relationships that could have appeared to influence the work reported in this paper.

Acknowledgments

The study was financed by the Engineering and Physical Sciences Research Council (EPSRC) grant no. EP/T026197/1, EP/W028786/1.

Data availability

Data for manuscript is available at: https://doi.org/10.5258/SOTON/D3107

References

1. G. K. Scadding, H. H. Kariyawasam, G. Scadding, R. Mirakian, R. J. Buckley, T. Dixon, S. R. Durham, S. Farooque, N. Jones, S. Leech, S. M. Nasser, R. Powell, G. Roberts, G. Rotiroti, A. Simpson, H. Smith, and A. T. Clark, "BSACI guideline for the diagnosis and management of allergic and non-allergic rhinitis (Revised Edition 2017; First edition 2007)," Clinical & Experimental Allergy **47**(7), 856–889 (2017).

2. K. B. Leth-Møller, T. Skaaby, and A. Linneberg, "Allergic rhinitis and allergic sensitisation are still increasing among Danish adults," Allergy **75**(3), 660–668 (2020).

3. X. Li, X. Xu, J. Li, Y. Huang, C. Wang, Y. Zhang, and L. Zhang, "Direct and indirect costs of allergic and non-allergic rhinitis to adults in Beijing, China," Clin Transl Allergy **12**(4), e12148 (2022).

4. V. Bauchau and S. R. Durham, "Prevalence and rate of diagnosis of allergic rhinitis in Europe," European Respiratory Journal **24**(5), 758–764 (2004).

5. N. J. Osborne, I. Alcock, B. W. Wheeler, S. Hajat, C. Sarran, Y. Clewlow, R. N. McInnes, D. Hemming, M. White, S. Vardoulakis, and L. E. Fleming, "Pollen exposure and hospitalization due to asthma exacerbations: daily time series in a European city," Int J Biometeorol **61**(10), 1837–1848 (2017).

6. D. Caillaud, S. Martin, C. Segala, J.-P. Besancenot, B. Clot, and M. Thibaudon, "Effects of Airborne Birch Pollen Levels on Clinical Symptoms of Seasonal Allergic Rhinoconjunctivitis," Int Arch Allergy Immunol **163**(1), 43–50 (2014).

7. R. Sousa-Silva, A. Smargiassi, D. Kneeshaw, J. Dupras, K. Zinszer, and A. Paquette, "Strong variations in urban allergenicity riskscapes due to poor knowledge of tree pollen allergenic potential," Sci Rep **11**(1), 10196 (2021).

8. R. M. Newnham, T. H. Sparks, C. A. Skjøth, K. Head, B. Adams-Groom, and M. Smith, "Pollen season and climate: Is the timing of birch pollen release in the UK approaching its limit?," Int J Biometeorol **57**(3), 391–400 (2013).

9. T. Suchan, G. Talavera, L. Sáez, M. Ronikier, and R. Vila, "Pollen metabarcoding as a tool for tracking long-distance insect migrations.," Mol Ecol Resour **19**(1), 149–162 (2019).

10. P. C. Fernandez-Mensaque, F. J. G. Minero, J. Morales, and C. Tomas, "Forecasting olive (Olea europaea) crop production by monitoring airborne pollen," Aerobiologia (Bologna) **14**(2), 185–190 (1998).

11. J. A. Grant-Jacob and B. Mills, "Deep learning in airborne particulate matter sensing: a review," J Phys Commun **6**(12), 122001 (2022).

12. E. Levetin, C. A. Rogers, and S. A. Hall, "Comparison of pollen sampling with a Burkard Spore Trap and a Tauber Trap in a warm temperate climate," Grana **39**(6), 294–302 (2000).

13. C. H. Pashley, J. Satchwell, and R. E. Edwards, "Ragweed pollen: is climate change creating a new aeroallergen problem in the UK?," (2015).

14. K. Warcup, B. Roberton, K. Kral-O'Brien, and J. Harmon, "Acetolysis modifications to process small pollen samples swabbed from live bees," Journal of Insect Science **23**(6), 1 (2023).

15. M. P. Alexander, "A versatile stain for pollen fungi, yeast and bacteria," Stain Technol **55**(1), 13–18 (1980).

16. B. Zimmermann and A. Kohler, "Infrared Spectroscopy of Pollen Identifies Plant Species and Genus as Well as Environmental Conditions," PLoS One **9**(4), e95417- (2014).

17. W. Sickel, M. J. Ankenbrand, G. Grimmer, A. Holzschuh, S. Härtel, J. Lanzen, I. Steffan-Dewenter, and A. Keller, "Increased efficiency in identifying mixed pollen samples by meta-barcoding with a dual-indexing approach," BMC Ecol **15**(1), 20 (2015).

18. S. Kawashima, M. Thibaudon, S. Matsuda, T. Fujita, N. Lemonis, B. Clot, and G. Oliver, "Automated pollen monitoring system using laser optics for observing seasonal changes in the concentration of total airborne pollen," Aerobiologia (Bologna) **33**(3), 351–362 (2017).

19. J. Schiele, F. Rabe, M. Schmitt, M. Glaser, F. Haring, J. O. Brunner, B. Bauer, B. Schuller, C. Traidl-Hoffmann, and A. Damialis, "Automated Classification of Airborne Pollen using Neural Networks," in *2019 41st Annual International Conference of the IEEE Engineering in Medicine and Biology Society (EMBC)* (2019), **2019**, pp. 4474–4478.

20. B. Crouzy, M. Stella, T. Konzelmann, B. Calpini, and B. Clot, "All-optical automatic pollen identification: Towards an operational system," Atmos Environ **140**, 202–212 (2016).

21. K. Mitsumoto, K. Yabusaki, and H. Aoyagi, "Classification of pollen species using autofluorescence image analysis," J Biosci Bioeng **107**(1), 90–94 (2009).

22. J. A. Grant-Jacob, Y. Xie, B. S. Mackay, M. Praeger, M. D. T. McDonnell, D. J. Heath, M. Loxham, R. W. Eason, and B. Mills, "Particle and salinity sensing for the marine environment via deep learning using a Raspberry Pi," Environ Res Commun **1**(3), 035001 (2019).

23. C. F. Bohren and D. R. Huffman, *Absorption and Scattering of Light by Small Particles* (John Wiley & Sons, 2008).

24. W. J. Wiscombe, "Improved Mie scattering algorithms," Appl Opt **19**(9), 1505–1509 (1980).

25. A. M. Maiden, M. J. Humphry, F. Zhang, and J. M. Rodenburg, "Superresolution imaging via ptychography," JOSA A **28**(4), 604–612 (2011).

26. J. R. Fienup, "Phase retrieval algorithms: a comparison," Appl Opt **21**(15), 2758–2769 (1982).

27. F. Pfeiffer, T. Weitkamp, O. Bunk, and C. David, "Phase retrieval and differential phase-contrast imaging with low-brilliance X-ray sources," Nat Phys **2**, 258–261 (2006).

28. J. A. Grant-Jacob, M. Praeger, M. Loxham, R. W. Eason, and B. Mills, "Lensless imaging of pollen grains at three-wavelengths using deep learning," Environ Res Commun **2**(7), 075005 (2020).

29. T. Nguyen, Y. Xue, Y. Li, L. Tian, and G. Nehmetallah, "Deep learning approach for Fourier ptychography microscopy," Opt. Express **26**(20), 26470–26484 (2018).

30. A. Goy, K. Arthur, S. Li, and G. Barbastathis, "Low photon count phase retrieval using deep learning," Phys Rev Lett **121**(24), 243902 (2018).

31. Z. D. C. Kemp, "Propagation based phase retrieval of simulated intensity measurements using artificial neural networks," Journal of Optics **20**(4), 45606 (2018).

32. K. W. Griener and S. Warny, "Nothofagus pollen grain size as a proxy for long-term climate change: An applied study on Eocene, Oligocene, and Miocene sediments from Antarctica," Rev Palaeobot Palynol **221**, 138–143 (2015).

33. T.-C. Lau, X. Lu, R. T. Koide, and A. G. Stephenson, "Effects of soil fertility and mycorrhizal infection on pollen production and pollen grain size of Cucurbita pepo (Cucurbitaceae)," Plant Cell Environ **18**(2), 169–177 (1995).

34. J. A. Grant-Jacob, B. S. Mackay, J. A. G. Baker, D. J. Heath, Y. Xie, M. Loxham, R. W. Eason, and B. Mills, "Real-time particle pollution sensing using machine learning," Opt. Express **26**(21), 27237–27246 (2018).

35. J. A. Grant-Jacob, S. Jain, Y. Xie, B. S. Mackay, M. D. T. McDonnell, M. Praeger, M. Loxham, D. J. Richardson, R. W. Eason, and B. Mills, "Fibre-optic based particle sensing via deep learning," Journal of Physics: Photonics **1**(4), 44004 (2019).

36. J. A. Grant-Jacob, Y. Xie, B. S. Mackay, M. Praeger, M. D. T. McDonnell, D. J. Heath, M. Loxham, R. W. Eason, and B. Mills, "Particle and salinity sensing for the marine environment via deep learning using a Raspberry Pi," Environ Res Commun **1**(3), 35001 (2019).

37. C. Li, M. Polling, L. Cao, B. Gravendeel, and F. J. Verbeek, "Analysis of automatic image classification methods for Urticaceae pollen classification," Neurocomputing **522**, 181–193 (2023).

38. M. Polling, C. Li, L. Cao, F. Verbeek, L. A. de Weger, J. Belmonte, C. De Linares, J. Willemse, H. de Boer, and B. Gravendeel, "Neural networks for increased accuracy of allergenic pollen monitoring," Sci Rep **11**(1), (2021).

39. P. Isola, J.-Y. Zhu, T. Zhou, and A. A. Efros, "Image-to-Image Translation with Conditional Adversarial Networks," in *2017 IEEE Conference on Computer Vision and Pattern Recognition (CVPR)* (IEEE, 2017), pp. 5967–5976.

40. J. A. Grant-Jacob, C. Everitt, R. W. Eason, L. J. King, and B. Mills, "Exploring sequence transformation in magnetic resonance imaging via deep learning using data from a single asymptomatic patient," J Phys Commun **5**(9), 95015 (2021).

41. N. Venkatanath, D. Praneeth, M. C. Bh, S. S. Channappayya, and S. S. Medasani, "Blind image quality evaluation using perception based features," in *2015 Twenty First National Conference on Communications (NCC)* (2015), pp. 1–6.

42. Y. Wang and J. F. Muth, "An Optical-Fiber-Based Airborne Particle Sensor," Sensors (Basel) **17**(9), 2110 (2017).

43. Y. Luo, Y. Zhang, T. Liu, A. Yu, Y. Wu, and A. Ozcan, "Virtual Impactor-Based Label-Free Pollen Detection using Holography and Deep Learning," ACS Sens **7**(12), 3885–3894 (2022).